

# Baryon spectra and non-strange baryon strong decays in the chiral SU(3) quark model

H.M. Zhao<sup>1</sup>, P.N. Shen<sup>5,1,4</sup>, Y.B. Ding<sup>2</sup>, X.Q. Li<sup>3,4</sup>, and B.S. Zou<sup>1,4,5</sup>

<sup>1</sup>*Institute of High Energy Physics, Chinese Academy of Sciences, P.O.Box 918(4), Beijing 100049, China*

<sup>2</sup>*Department of Physics, Graduate University of Chinese Academy of Sciences, Beijing 100049, China*

<sup>3</sup>*Department of Physics, Nankai University, Tianjin 300071, China*

<sup>4</sup>*Institute of Theoretical Physics, Chinese Academy of Sciences, P.O.Box 2735, China*

<sup>5</sup>*Center of Theoretical Nuclear Physics, National Laboratory of Heavy Ion Accelerator, Lanzhou 730000, China*

(Dated: July 3, 2021)

In the framework chiral SU(3) quark model, the baryon spectra within the band of  $N \leq 2$  are studied, and the effect of the confining potential in different configurations, namely the  $\Delta$ -mode and Y-mode are compared. In the same way, the baryon spectra in the extended chiral SU(3) quark model, in which additional vector meson exchanges are introduced, are also calculated. It is shown that a reasonable baryon spectrum in the chiral SU(3) quark model can be achieved no matter whether the  $\Delta$ -mode or the Y-mode confining potential is employed. In the extended chiral SU(3) quark model, several energy levels are further improved. The resultant binding energies of excited baryon states in different confining modes deviate just by a few to several tens MeV, and it is hard to justify which confining mode is the dominant one. The non-strange baryon strong decay widths are further discussed in the point-like meson emission model by using the wave-function obtained in the spectrum calculation. The resultant widths can generally explain the experimental data but still cannot distinguish which confining mode is more important in this simple decay mode.

PACS numbers: 13.75.Jz, 12.39.-x, 21.45.+v

Keywords: Quark model; Chiral symmetry

## I. INTRODUCTION

In the framework of the chiral SU(3) quark model [2], which is extropolated from the SU(2) linear  $\sigma$  model [1], a unified description of the experimental data on the masses of the baryon ground states, the binding energy of deuteron, and the baryon-baryon scattering has successfully been achieved [2, 3, 4]. Later, this model has been applied to the study of multi-quark systems to predict new dibaryons and explain newly observed hadron states [5, 6]. Whether this model can also describe the baryon spectrum in a reasonable extent would be one more place to confirm the

reliability of the model in studying the hadron structure and the hadron-hadron scattering in the quark degrees of freedom.

In the chiral SU(3) quark model, the short range perturbative effect of QCD is generally characterized by the one-gluon-exchange (OGE) potential, the medium range non-perturbative effect of QCD is mainly described by one-Goldstone-bosons exchange (OBE) potentials, and the long distance non-perturbative effect is commonly depicted by a phenomenal confining potential, say a harmonic confinement potential.

In terms of the OGE quark model, we calculated the baryons spectra with different confining potential modes [7], and such potentials were derived from the flux tube model [8, 9] and later were confirmed by lattice QCD (LQCD) calculations [10]. For the baryon system, there exist two confining modes. In the first mode, called  $\Delta$ -mode, the confining potential can approximately be described by a sum of two-body confining potentials. The second mode associates with a genuine three-body interaction, called Y-mode. In recent years, with the development of the fast computer, more and more LQCD calculations on three-quark potential have been carried out. Typical works on this aspect are done by Takahashi *et al.*[11] and Alexandrou *et al.*[14]. Takahashi *et al.* more accurately considered three quark Wilson loops and advocated that the Y-shape confining mode is the dominant confining mode in baryon. But, Alexandrou *et al.* believed that the  $\Delta$ -mode is favored at least in the distances smaller than  $1.2fm$ . Different from other works [12, 15, 16, 17, 18], we respectively calculated the contributions of these two confining potential modes directly, and found that by employing either the  $\Delta$ -mode or Y-mode confining potential, one can achieve reasonable baryon spectra in OGE quark model [7]. In this paper we evaluate the spectra and decay properties of baryons with these two confining modes in the chiral SU(3) quark model, and hope that which confining mode is more important in baryon can be explored.

In the next section, the baryon spectrum in the chiral SU(3) quark model is discussed and the effect of different confining modes is compared. The baryon spectrum in the extended chiral SU(3) quark model is further examined in section III, and in section IV the decays of baryons are calculated in a point-like meson emission model. Finally, the conclusion is drawn in section V.

## II. BARYON SPECTRUM IN CHIRAL SU(3) QUARK MODEL

### A. Brief formulism

In the chiral SU(3) quark model [2], the interaction induced by the chiral field describes the non-perturbative QCD effect in the medium distance. The interacting Hamiltonian between the quark and the chiral field can be written as

$$H_I^{ch} = g_{ch} F(q^2) \bar{\psi} \left( \sum_{a=0}^8 \sigma_a \lambda_a + i \sum_{a=0}^8 \pi_a \lambda_a \gamma_5 \right) \psi, \quad (1)$$

where  $g_{ch}$  is the coupling constant between the quark and the chiral-field,  $\lambda_0$  is a unitary matrix,  $\lambda_1, \dots, \lambda_8$  are the Gell-Mann matrix of the flavor SU(3) group,  $\sigma_0, \dots, \sigma_8$  denote the scalar singlet and octet fields and  $\pi_0, \dots, \pi_8$  represent the pseudoscalar singlet and octet fields, respectively.  $F(q^2)$  is a form factor to describe the chiral-field structure [19, 20] and, as usual, is taken as

$$F(q^2) = \left( \frac{\Lambda^2}{\Lambda^2 + q^2} \right)^{1/2}, \quad (2)$$

where  $\Lambda$  is the cutoff mass of the chiral field. It can be verified that  $H_I^{ch}$  is invariant under the infinitesimal chiral SU(3) transformation.

With  $H_I^{ch}$ , the chiral-field-induced effective quark-quark potentials can be written as:

$$V_{ij}^{ch} = \sum_{a=0}^8 V_{\sigma_a}(r_{ij}) + \sum_{a=0}^8 V_{\pi_a}(r_{ij}), \quad (3)$$

where

$$V_{\sigma_a}(r_{ij}) = -C(g_{ch}, m_{\sigma_a}, \Lambda) X_1(m_{\sigma_a}, \Lambda, r_{ij}) [\lambda_a(i) \lambda_a(j)] + V_{\sigma_a}^{l-s}(r_{ij}), \quad (4)$$

$$V_{\pi_a}(r_{ij}) = C(g_{ch}, m_{\pi_a}, \Lambda) \frac{m_{\pi_a}^2}{12m_{q_i}m_{q_j}} X_2(m_{\pi_a}, \Lambda, r_{ij}) (\sigma_i \cdot \sigma_j) [\lambda_a(i) \lambda_a(j)] + V_{\pi_a}^{ten}(r_{ij}), \quad (5)$$

and

$$V_{\sigma_a}^{l-s}(r_{ij}) = -C(g_{ch}, m_{\sigma_a}, \Lambda) \frac{m_{\sigma_a}^2}{4m_{q_i}m_{q_j}} \left\{ G(m_{\sigma_a} r_{ij}) - \left( \frac{\Lambda}{m_{\sigma_a}} \right)^3 G(\Lambda r_{ij}) \right\} \\ \times [L \cdot (\sigma_i + \sigma_j)] [\lambda_a(i) \lambda_a(j)], \quad (6)$$

$$V_{\pi_a}^{ten}(r_{ij}) = C(g_{ch}, m_{\pi_a}, \Lambda) \frac{m_{\pi_a}^2}{12m_{q_i}m_{q_j}} \left\{ H(m_{\pi_a} r_{ij}) - \left( \frac{\Lambda}{m_{\pi_a}} \right)^3 H(\Lambda r_{ij}) \right\} \\ \times [3(\sigma_i \cdot \hat{r}_{ij})(\sigma_j \cdot \hat{r}_{ij}) - \sigma_i \cdot \sigma_j] [\lambda_a(i) \lambda_a(j)], \quad (7)$$

with

$$C(g_{ch}, m, \Lambda) = \frac{g_{ch}^2}{4\pi} \frac{\Lambda^2}{\Lambda^2 - m^2} m, \quad (8)$$

$$X_1(m, \Lambda, r) = Y(mr) - \frac{\Lambda}{m} Y(\Lambda r), \quad (9)$$

$$X_2(m, \Lambda, r) = Y(mr) - \left(\frac{\Lambda}{m}\right)^3 Y(\Lambda r), \quad (10)$$

$$Y(x) = \frac{1}{x} e^{-x}, \quad (11)$$

$$G(x) = \frac{1}{x} \left(1 + \frac{1}{x}\right) Y(x), \quad (12)$$

$$H(x) = \left(1 + \frac{3}{x} + \frac{3}{x^2}\right) Y(x), \quad (13)$$

and  $m_{\sigma_a}$  and  $m_{\pi_a}$  being the masses of the scalar meson and the pseudoscalar meson, respectively.

The short-range interaction in the model is mainly governed by the one-gluon-exchange interaction

$$V_{ij}^{OGE} = \frac{1}{4} g_i g_j (\lambda_i^c \cdot \lambda_j^c) \left\{ \frac{1}{r_{ij}} - \frac{\pi}{2} \delta(r_{ij}) \left( \frac{1}{m_{q_i}^2} + \frac{1}{m_{q_j}^2} + \frac{4}{3} \frac{1}{m_{q_i} m_{q_j}} (\sigma_i \cdot \sigma_j) \right) \right\} + V_{OGE}^{l.s}, \quad (14)$$

with

$$V_{OGE}^{l.s} = -\frac{1}{16} g_i g_j (\lambda_i^c \cdot \lambda_j^c) \frac{3}{m_{q_i} m_{q_j}} \frac{1}{r_{ij}^3} L \cdot (\sigma_i + \sigma_j). \quad (15)$$

For the interaction in the long-distance range, confining potential dominates the behavior of the system. In this paper, two kinds of confining modes are considered. The  $\Delta$ -mode confining potential of a three quark system can generally be written as:

$$V_{\Delta}^{conf} = \frac{1}{2} b \sum_{i < j} r_{ij} + C_{\Delta}, \quad (16)$$

where  $b$  denotes the string tension,  $C_{\Delta}$  is an overall constant. The Y-mode confining potential is related to the energy of the flux tube connecting three valance quarks, and the total length of the flux tube should take the minimal value for stability. The general form of the Y-mode confining potential is written as [12]

$$V_Y^{conf} = b \sum_{i=1}^3 |\mathbf{r}_i - \mathbf{r}_0| + C_Y, \quad (17)$$

where  $C_Y$  is an overall constant, and  $\mathbf{r}_0$  is the coordinate of the junction point. The rule for finding the location of the junction point is the following: If all the inner angles of the triangle with three constituent quarks sitting at the apexes of the triangle are smaller than  $2\pi/3$ , the junction point is located inside the triangle and the angles spanned by two flux tubes are  $2\pi/3$ . If one of the inner angles of the triangle would take a value equal to or greater than  $2\pi/3$ , the junction point would be located at that apex. Let the lengths of the three sides of the triangle be  $a$ ,  $b$  and  $c$ , respectively.  $L_{min}$  then can be expressed as [11, 12, 13]

$$L_{min} = \begin{cases} \left[ \frac{1}{2}(a^2 + b^2 + c^2) + \frac{\sqrt{3}}{2} \sqrt{(a+b+c)(-a+b+c)(a-b+c)(a+b-c)} \right]^{1/2} \\ \quad \text{if all the inner angles are smaller than } 2\pi/3, \\ \\ a + b + c - \max(a, b, c) \\ \quad \text{if one of the inner angles is not smaller than } 2\pi/3. \end{cases} \quad (18)$$

For the baryon systems, the total Hamiltonian can be written as

$$H = \sum_{i=1}^3 T_i - T_G + \sum_{i<j=1}^3 V_{ij} + V^{conf}, \quad (19)$$

with

$$V_{ij} = V_{ij}^{OGE} + V_{ij}^{ch}. \quad (20)$$

Where  $T_i$  and  $T_G$  are the kinetic energy operators of the  $i$ -th quark and the center of mass, respectively. The kinetic energy operator in the semi-relativistic form is

$$T_i = \sum_{i=1}^3 \sqrt{p_i^2 + m_i^2}. \quad (21)$$

As a physical baryon  $B$ , it has a certain spin  $(J, J_Z)$  and a certain parity  $(P)$ , where  $J$  and  $J_Z$  represent the quantum number of the total angular momentum  $\mathbf{J} = \mathbf{L} + \mathbf{S}$  and its magnetic quantum number, respectively, and  $P = (-1)^L$ . Therefore, the wave function of the baryon  $B$  with quantum number  $J^P$  should be constructed as

$$|J, J_Z, P, B\rangle = \Phi^C \sum_{M=-L}^L \sum_{S_Z} (J, J_Z | L, M, S, S_Z) \phi_B^{SF}(S, S_Z, \xi, \Sigma_B^{SF}) \psi_{L,M}^N(\eta, \zeta, \Sigma^O), \quad (22)$$

where  $(J, J_Z | L, M, S, S_Z)$  is the CG coefficient for L-S coupling,  $\Phi^C$  denotes the total color wave function which should be totally antisymmetric,  $\phi_B^{SF}(S, S_Z, \xi, \Sigma_B^{SF})$  represents the  $SU_{SF}(6)$  spin and flavor wave functions,  $\psi_{L,M}^N(\eta, \zeta, \Sigma^O)$  is the spatial wave function with  $N = 2(n_\rho + n_\lambda) + l_\rho + l_\lambda$

being the principal quantum number,  $L$  and  $M$  being the quantum number of the total orbital angular momentum  $\mathbf{L} = \mathbf{l}_\rho + \mathbf{l}_\lambda$  and its magnetic quantum number, respectively,  $\Sigma^O$  standing for the symmetry of the spatial wave function,  $\eta$  being the width parameter and  $\zeta$  representing the aggregate of the spatial variables, and  $\phi_B^{SF}(S, S_Z, \xi, \Sigma_B^{SF})$  and  $\psi_{L,M}^N(\eta, \zeta, \Sigma^O)$  must be coupled to a symmetric wave function. The detailed forms of these wave functions can be found in Ref. [21, 22].

The baryon spectrum is solved by using the variational method. The matrix element of kinetic energy operator (21) is calculated in the momentum space [12]. According to the definitions of the coordinates

$$\begin{aligned}\mathbf{R} &= \frac{m_1\mathbf{r}_1 + m_2\mathbf{r}_2 + m_3\mathbf{r}_3}{m_1 + m_2 + m_3} \\ \rho &= \frac{1}{\sqrt{2}}(\mathbf{r}_1 - \mathbf{r}_2) \\ \lambda &= \sqrt{\frac{2}{3}}\left(\frac{m_1\mathbf{r}_1 + m_2\mathbf{r}_2}{m_1 + m_2} - \mathbf{r}_3\right),\end{aligned}\tag{23}$$

the momenta in the rest frame are related to those in the center of mass frame by

$$\begin{aligned}\mathbf{p}_1 &= \frac{1}{\sqrt{2}}\mathbf{p}_\rho + \frac{1}{\sqrt{6}}\mathbf{p}_\lambda, \\ \mathbf{p}_2 &= -\frac{1}{\sqrt{2}}\mathbf{p}_\rho + \frac{1}{\sqrt{6}}\mathbf{p}_\lambda, \\ \mathbf{p}_3 &= -\frac{2}{\sqrt{6}}\mathbf{p}_\lambda.\end{aligned}\tag{24}$$

The detailed evaluation of the matrix elements can be found in Ref. [7] and references therein. In our numerical calculation, the spin-orbital interaction is dropped out due to the weakness of such an interaction showing in the experimental data of the baryon spectrum.

## B. Determination of parameters

There are four initial input parameters: the up (down) quark mass  $m_{u(d)}$ , the strange quark mass  $m_s$ , the harmonic oscillator frequency  $\omega$  and the confining strength  $b$ . The up (down) quark mass  $m_{u(d)}$  and the strange quark mass  $m_s$  are taken to be commonly used values of  $330MeV$  and  $470MeV$ , respectively.  $\omega$  is chosen to be  $0.497 GeV$ , which will produce a radius of about  $0.5fm$  for a bare nucleon. The string tension is chosen, according to the LQCD result [11], to be  $0.20GeV^{-1}$  for the Y-mode and an additional factor of 0.53 for the  $\Delta$ -mode. The other model parameters are fixed in the following way. The chiral coupling constant  $g_{ch}$  is fixed by

$$\frac{g_{ch}^2}{4\pi} = \left(\frac{3}{5}\right)^2 \frac{g_{NN\pi}^2}{4\pi} \frac{m_u^2}{M_N^2},\tag{25}$$

with  $g_{NN\pi}^2/4\pi = 13.67$  being the empirical value. The masses of exchanged mesons are adopted from the experimental data, except for the  $\sigma$  meson. In our calculation, the mass of  $\sigma$  is a free parameter and its value of 675 MeV is determined by the best fit to the experimental data available [2, 4]. The cutoff momentum  $\Lambda$  is taken to be close to the chiral symmetry breaking scale [19, 20]. After the parameters of chiral fields are fixed, the one gluon exchange coupling constants  $g_u$  and  $g_s$  can be determined by the mass splittings between  $N$  and  $\Delta$  and between  $\Sigma$  and  $\Lambda$ , respectively. The zero point energies  $C^{uu}$ ,  $C^{us}$  and  $C^{ss}$  in the  $\Delta$ -mode confining potential are fixed by the masses of the ground state baryons  $N$ ,  $\Lambda$  and the average masses of  $\Xi$  and  $\Omega$ , respectively. And the zero point energies  $C^N$ ,  $C^\Lambda = C^\Sigma$ ,  $C^\Xi$  and  $C^\Omega$  in the Y-mode confining potential case are fixed by the masses of  $N$ ,  $\Lambda$ ,  $\Xi$  and  $\Omega$ , respectively.

In the calculation,  $\eta$  and  $\eta'$  mesons are mixed by  $\eta_1$  and  $\eta_8$  with a mixing angle  $\theta^{PS}$  of  $-23^\circ$  as usual. The mixing angle  $\theta^S$  between  $\sigma_0$  and  $\sigma_8$  is still an open issue because the structure of  $\sigma$  meson is unclear and controversial.  $35.264^\circ$  is adopted from Ref. [4] which indicates that  $\sigma$  and  $\epsilon$  are ideally mixed by  $\sigma_0$  and  $\sigma_8$ .

The resultant model parameters are tabulated in Table I.

### C. Baryon spectrum

In the chiral SU(3) quark model, the baryon spectra for  $N \leq 2$  bands with  $\Delta$ -mode and Y-mode confining potentials are calculated. The non-strange baryon spectra in  $N \leq 2$  bands are plotted in Fig. 1 and also tabulated in Table II. In this figure, the solid and dashed bars denote the results in the  $\Delta$ -confining mode and in the Y-confining mode, respectively. It is shown that no matter which confining mode is employed, most of resultant resonances are fairly well located within experimental errors. The differences of resultant resonances by using different confining modes are rather small and most of them are in several tens MeV to several MeV. For comparison, the results by using the so-called relativistic quark model [12], where the semi-relativistic corrections were considered and the OGE and confining potentials were employed only, are also given in Fig. 2. Comparing with Fig. 2, in our model, most resonances in positive-parity sector, except  $\Delta^*(\frac{3}{2}^+, 1600)$  which is 200 MeV higher than the experimental center value, can be fitted to the experimental data much better. The reason for worse fitting of  $\Delta^*(\frac{3}{2}^+, 1600)$  can be attributed to the fact that the contribution of the contact term for this state is much larger than that for the other states in this band (referring to the hyperfine matrix elements in the table in Ref.[24]). To avoid the singular behavior of the wave function at the origin due to the  $\delta(\mathbf{r})$  function in the contact term in the

TABLE I: Model parameters. The meson masses and the cutoff masses are taken to be  $m_{\sigma'} = 980$  MeV,  $m_{\kappa} = 980$  MeV,  $m_{\epsilon} = 980$  MeV,  $m_{\pi} = 138$  MeV,  $m_K = 495$  MeV,  $m_{\eta} = 549$  MeV,  $m_{\eta'} = 957$  MeV,  $\Lambda = 1100$  MeV.

	$\Delta$ -shape	Y-shape
$g_u$	0.900	0.900
$g_s$	0.955	0.955
$b_{\Delta}^{uu}(GeV/fm)$	1.01	-
$b_{\Delta}^{us}(GeV/fm)$	1.01	-
$b_{\Delta}^{ss}(GeV/fm)$	1.01	-
$C_{\Delta}^{uu}(MeV)$	-1053	-
$C_{\Delta}^{us}(MeV)$	-936	-
$C_{\Delta}^{ss}(MeV)$	-751	-
$b_Y^N(GeV/fm)$	-	0.91
$b_Y^{\Lambda}(GeV/fm)$	-	1.01
$b_Y^{\Xi}(GeV/fm)$	-	1.01
$b_Y^{\Omega}(GeV/fm)$	-	1.01
$C_Y^N(MeV)$	-	-1170
$C_Y^{\Lambda}(MeV)$	-	-1085
$C_Y^{\Xi}(MeV)$	-	-989
$C_Y^{\Omega}(MeV)$	-	-213

potential, the authors of Ref. [12] employed a smearing factor and also included the relativistic corrections for the terms related to the quark mass. As a consequence, the mass of  $\Delta^*(\frac{3}{2}^+, 1600)$  in their calculation is smaller than ours but is still higher than the upper limit of experimental error bar. For the negative parity sector, our results are similar to Ref.[12], and our  $N^*(\frac{1}{2}^+, 1650)$  fits the experimental data much better. Our resultant mass of the Roper resonance ( $N^*(\frac{1}{2}^+, 1440)$ ) is still higher than that of the first orbital resonance  $N^*(\frac{1}{2}^-, 1535)$ , which is similar to the predictions in Ref.[12]. In recent years, some one argued that the Roper resonance is not a pure baryon [25].

The baryon spectra with strange number  $S = -1$  in  $N \leq 2$  bands are given in Table III-IV and Fig.3. Once again, the results of Ref. [12] are pictured in Fig. 4. From Fig. 3, one sees that the fitting quality of spectra to the experimental data in this sector is not as good as that in the non-strange sector, but most of the resultant resonances are located within experimental error bars. In general, the fitting quality is similar to that in Ref. [12]. The spectra with the  $\Delta$ -mode



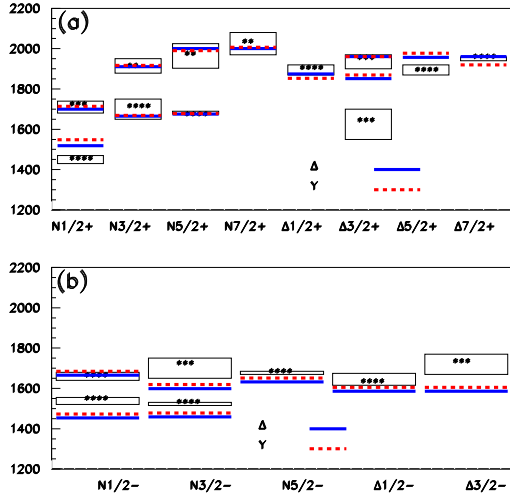


FIG. 1: The non-strange baryon in  $N \leq 2$  bands in the chiral  $SU(3)$  quark model. Boxes show the experimental regions of the resonances. The solid and dashed bars represent the results in the  $\Delta$ -mode case and in the Y-mode case, respectively.

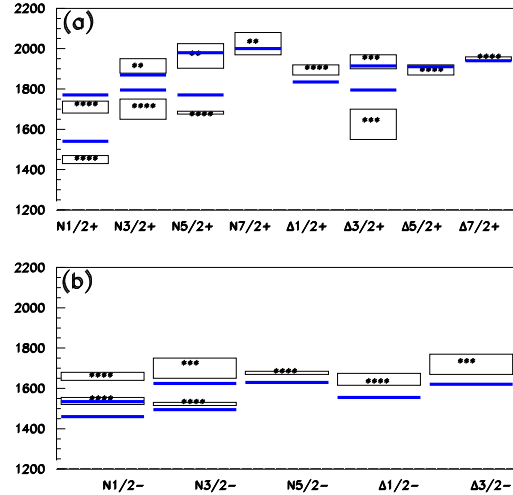


FIG. 2: The non-strange baryon spectra in  $N \leq 2$  bands in Ref.[12]. Boxes show the experimental regions of the resonances. The solid and dashed bars represent the results in the  $\Delta$ -mode case and in the Y-mode case, respectively.

confining potential is close to those with the Y-mode, just as that in the non-strange sector. The evaluated mass of  $\Lambda^*(\frac{1}{2}^-, 1405)$  is more than 100 MeV larger than the experimental value when the spin-orbit interaction, which causes the mass splitting between  $\Lambda^*(\frac{1}{2}^-, 1405)$  and  $\Lambda^*(\frac{3}{2}^-, 1520)$ , is omitted in the calculation. Inclusion of such an interaction would result in a more reasonable spectrum for strange baryons Ref. [26].

The  $S = -2$  and  $-3$  baryon spectra in  $N \leq 2$  bands are given in Fig. 5 and Table V. The deviations of the results with the Y-mode from those with  $\Delta$ -mode are similar to those in the former sectors. The results show that both the  $\Delta$ -mode and the Y-mode confining potentials can lead to reasonable baryon spectra.

#### D. Comparison of $\Delta$ -mode and Y-mode

In order to study the effect of different confinement modes on the baryon spectrum, we now use a confining potential in which both  $\Delta$ -mode and the Y-mode are included

$$V^{conf} = xV_{\Delta}^{conf} + (1-x)V_Y^{conf}, \quad (26)$$

where  $x$  stands for the fraction of the  $\Delta$ -mode in the whole confining potential. The  $S=0$  and  $-1$  baryon spectra with  $x$  values of 0.2, 0.5 and 0.8 are plotted in Figs. 6 and 7, respectively. The

TABLE II: Non-strange baryon masses in  $N \leq 2$  bands (in  $MeV$ ). Experimental data are taken from [23].

State	$\Delta$ -mode	Y-mode	experimental data	
$N^* \frac{1}{2}^+$	939	939	939	****
	1519	1548	1430-1470	****
	1700	1714	1680-1740	***
	1970	1961	1885-2125	*
	2063	2056		
$\Delta^* \frac{1}{2}^+$	1874	1853	1870-1920	****
	1949	1942		
$N^* \frac{3}{2}^+$	1665	1669	1650-1750	****
	1910	1917	1879-1951	**
	1977	1970		
	2051	2048		
	2357	2366		
$\Delta^* \frac{3}{2}^+$	1232	1232	1232	****
	1852	1870	1550-1700	***
	1961	1961	1900-1970	***
	2000	2024		
$N^* \frac{5}{2}^+$	1675	1678	1675-1690	****
	2001	1990	1903-2025	**
	2356	2365		
$\Delta^* \frac{5}{2}^+$	1957	1977	1870-1920	****
	2028	2020	1724-2200	**
$N^* \frac{7}{2}^+$	2000	2007	1970-2080	**
$\Delta^* \frac{7}{2}^+$	1961	1919	1940-1960	****
$N^* \frac{1}{2}^-$	1454	1473	1520-1555	****
	1665	1685	1640-1680	****
$\Delta^* \frac{1}{2}^-$	1586	1605	1615-1675	****
$N^* \frac{3}{2}^-$	1459	1478	1515-1530	****
	1599	1619	1650-1750	***
$\Delta^* \frac{3}{2}^-$	1586	1605	1670-1770	***
$N^* \frac{5}{2}^-$	1632	1652	1670-1685	****

resultant baryon spectra with different x-values show very small differences.

From the structure of the flux-tube model, the difference between the Y-mode and the  $\Delta$ -mode potentials comes from different geometric shapes of flux-tubes in baryon. By denoting  $L_Y$  and  $L_\Delta$  as the lengths of the Y-mode and  $\Delta$ -mode flux-tubes, respectively, we have

$$\frac{L_\Delta}{2} \leq L_Y \leq \frac{2}{\sqrt{3}} \frac{L_\Delta}{2}, \quad (27)$$

where the left equal sign means that the junction point is sitting at the apex and the right equal sign represents the fact that three quarks in baryon stay at apexes of an equilateral triangle. Further

TABLE III: Positive-parity S=-1 baryon masses in  $N \leq 2$  bands (in  $MeV$ ). Experimental data are taken from [23].

State	$\Delta$ -mode	Y-mode	experimental data	
$\Lambda^* \frac{1}{2}^+$	1115	1115	1115.6	****
	1690	1717	1560-1700	***
	1801	1814	1750-1850	***
	1844	1869		
	2088	2079		
	2127	2128		
	2173	2239		
$\Lambda^* \frac{3}{2}^+$ 1792	1727	1730	1850-1910	****
	2039	2066		
	2053	2072		
	2098	2090		
	2139	2196		
	2230	2265		
	2414	2323		
$\Lambda^* \frac{5}{2}^+$	1733	1735	1815-1825	****
	2092	2121	2090-2140	***
	2133	2187		
	2162	2207		
	2414	2423		
$\Lambda^* \frac{7}{2}^+$	2105	2115	2000-2140	*
$\Sigma^* \frac{1}{2}^+$	1192	1192	1192.6	****
	1759	1784	1630-1690	***
	1889	1918	1738-1790	*
	1992	1968	1826-1985	**
	2064	2060		
	2103	2092		
	2139	2220		
$\Sigma^* \frac{3}{2}^+$	1371	1370	1382	****
	1859	1854	1800-1925	*
	1995	2003	2070-2140	**
	2056	2060		
	2079	2092		
	2094	2096		
	2103	2124		
	2135	2212		
	2200	2221		
	$\Sigma^* \frac{5}{2}^+$	1868	1859	1900-1930
2065		2069	2050-2080	*
2099		2121		
2163		2217		
2199		2237		
$\Sigma^* \frac{7}{2}^+$	2062	2023	2025-2040	****
	2114	2204		

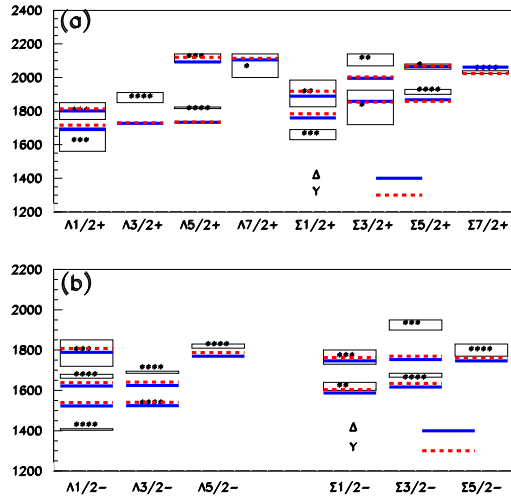


FIG. 3: The S=-1 baryon spectra in  $N \leq 2$  bands in the chiral SU(3) quark model. Legend as in Fig.1.

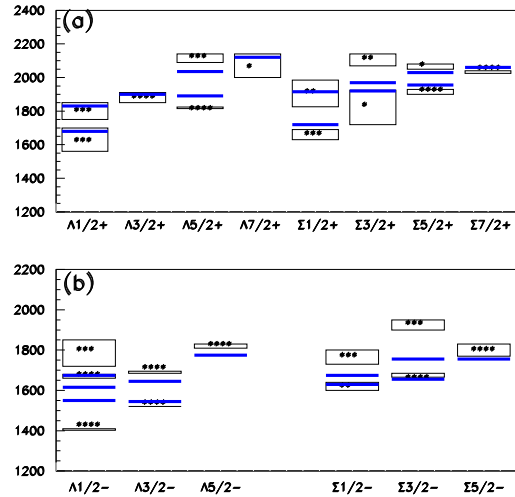


FIG. 4: The S=-1 baryon spectra in  $N \leq 2$  bands in [12]. Legend as in Fig.1.

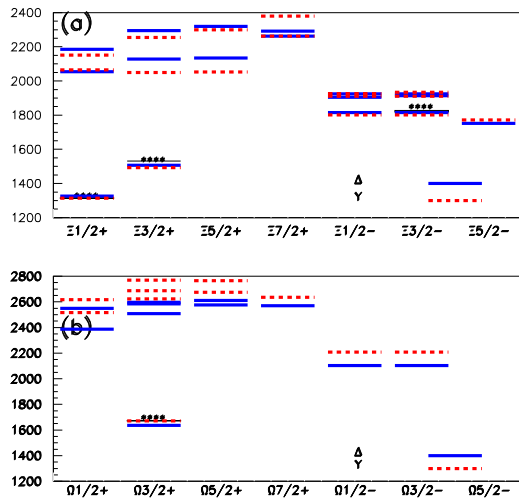


FIG. 5: The S=-2,-3 baryon spectra in  $N \leq 2$  bands in the chiral SU(3) quark model. Legend as in Fig.1.

considering a factor of  $\frac{1}{2}$  in the string tension of the  $\Delta$ -mode confining potential, the ratio of the Y-mode and  $\Delta$ -mode confining potentials satisfies

$$1 \leq \frac{L_Y}{L_{\Delta}/2} (= \frac{V_Y^{conf}}{V_{\Delta}^{conf}}) \leq \frac{2}{\sqrt{3}} \simeq 1.15. \quad (28)$$

This relation indicates that the maximal difference between the Y-mode and  $\Delta$ -mode confining potentials is 15%. Because the calculated baryon mass is closely related to the averaged values of potentials, one might not be able to distinguish the effects from two confining modes by studying the spectrum only. However, by carefully investigating the matrix element (ME) of the confining

TABLE IV: Negative-parity S=-1 baryon masses in N=1 bands (in  $MeV$ ). Experimental data are taken from [23].

State	$\Delta$ -mode	Y-mode	experimental data	
$\Lambda^* \frac{1}{2}^-$	1523	1540	1402-1410	****
	1622	1639	1660-1680	****
	1789	1808	1720-1850	****
$\Lambda^* \frac{3}{2}^-$	1524	1541	1518-1520	****
	1624	1641	1685-1695	****
	1748	1767	2307-2372	*
$\Lambda^* \frac{5}{2}^-$	1769	1788	1810-1830	****
$\Sigma^* \frac{1}{2}^-$	1587	1604	1600-1640	**
	1747	1763	1730-1800	***
	1774	1791	1755-2004	*
$\Sigma^* \frac{3}{2}^-$	1617	1635	1578-1584	**
	1743	1760	1665-1685	****
	1753	1769	1900-1950	***
$\Sigma^* \frac{5}{2}^-$	1746	1762	1770-1780	****

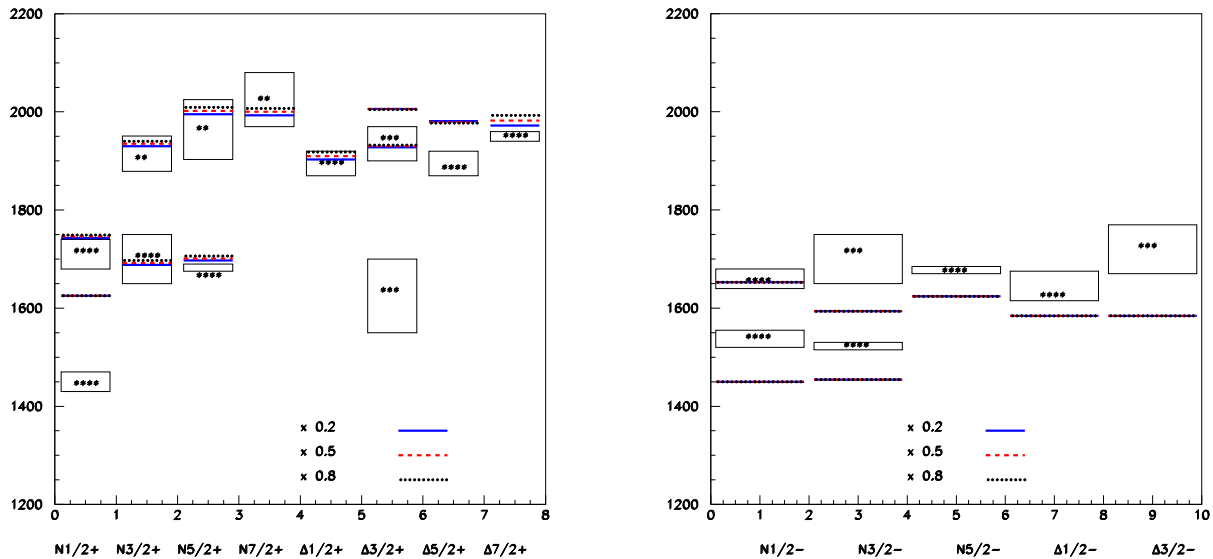


FIG. 6: S=0 baryon spectra with mixed  $\Delta$ - and Y-mode confining potentials in  $N \leq 2$  bands. The solid, dashed and dotted bars correspond to the results with  $x$  being 20%, 50% and 80%, respectively.

potential in different integrating intervals, one might see the different effects from different confining modes. In Fig. 8, we demonstrate the values of the matrix element of confining potentials in the Y-mode and  $\Delta$ -mode with respect to the quark separation step by step in several states. In this figure, the matrix element at  $r = \rho_{max} = \lambda_{max}$  with  $\rho_{max}$  and  $\lambda_{max}$  being the upper integrating limit of the  $\rho$  and  $\lambda$  integrations are normalized to 1 for an easy comparison. Evidently, at the short and medium distances ( $0.2fm - 0.8fm$ ), the  $\Delta$ -mode is dominant and at the large distances

TABLE V:  $\Xi$  and  $\Omega$  baryon masses in  $N \leq 2$  bands in the chiral SU(3) quark model (in  $MeV$ ). Experimental data are taken from [23].

State	Model	Predicted masses (MeV)								
$\Xi^* \frac{1}{2}^+$	$\Delta$ -shape	1327	1894	2016	2122	2190	2234	2263		
	Y-shape	1314	1907	2028	2085	2175	2212	2325		
$\Xi^* \frac{3}{2}^+$	$\Delta$ -shape	1506	1947	2122	2185	2204	2215	2234	2246	2361
	Y-shape	1493	1927	2115	2176	2204	2212	2232	2312	2367
$\Xi^* \frac{5}{2}^+$	$\Delta$ -shape	1952	2191	2218	2268	2361				
	Y-shape	1932	2177	2230	2327	2366				
$\Xi^* \frac{7}{2}^+$	$\Delta$ -shape	2184	2233							
	Y-shape	2134	2304							
$\Omega^* \frac{1}{2}^+$	$\Delta$ -shape	2262	2326							
	Y-shape	2516	2618							
$\Omega^* \frac{3}{2}^+$	$\Delta$ -shape	1636	2241	2339	2347					
	Y-shape	1672	2623	2688	2770					
$\Omega^* \frac{5}{2}^+$	$\Delta$ -shape	2333	2365							
	Y-shape	2674	2766							
$\Omega^* \frac{7}{2}^+$	$\Delta$ -shape	2322								
	Y-shape	2636								
$\Xi^* \frac{1}{2}^-$	$\Delta$ -shape	1756	1871	1890						
	Y-shape	1760	1875	1896						
$\Xi^* \frac{3}{2}^-$	$\Delta$ -shape	1756	1871	1896						
	Y-shape	1760	1875	1901						
$\Xi^* \frac{5}{2}^-$	$\Delta$ -shape	1892								
	Y-shape	1898								
$\Omega^* \frac{1}{2}^-$	$\Delta$ -shape	2104								
	Y-shape	2099								
$\Omega^* \frac{3}{2}^-$	$\Delta$ -shape	2104								
	Y-shape	2099								

the Y-mode provides more contributions. This result coincides with Alexandrou's argument [14]. Moreover, in lower lying states, the increase rate of the matrix element of the Y-mode potential is much slower than that of the  $\Delta$ -mode potential in the distances less than  $0.6fm$ , but becomes much faster as  $r > 0.8fm$ , especially in higher level states.

### III. THE EXTENDED CHIRAL SU(3) QUARK MODEL

Recently Zhang *et al* extended the chiral SU(3) quark model by including the exchanges of the singlet and octet vector meson fields between quarks. In this extended model, the vector meson

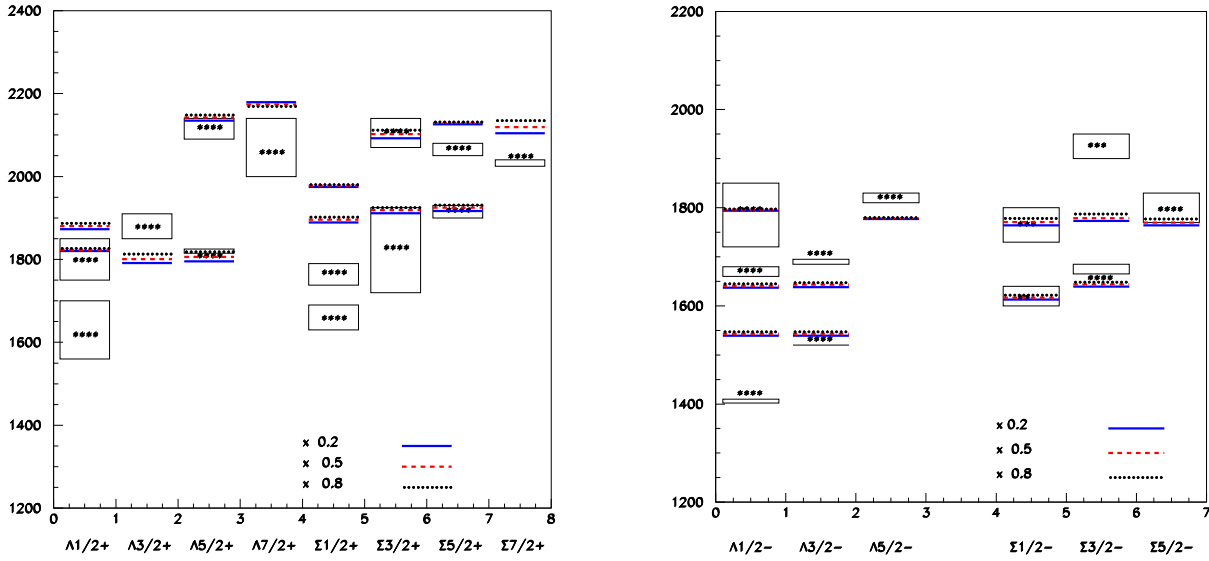


FIG. 7:  $S=-1$  baryon spectra with mixed  $\Delta$ - and  $Y$ -mode confining potentials in  $N \leq 2$  bands. The solid, dashed and dotted bars correspond to the results with  $x$  being 20%, 50% and 80%, respectively.

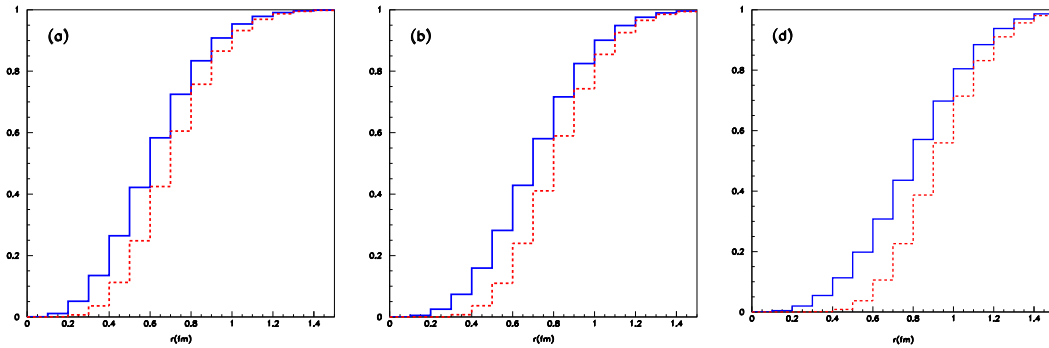


FIG. 8: Contributions of the matrix elements of  $\Delta$ -mode and  $Y$ -mode confining potentials with respect to the quark separation. (a)  $|^2N(56, 0^+)_{\frac{1}{2}^+} \rangle$  state, (b)  $|^2N(70, 1^-)_{\frac{1}{2}^-} \rangle$  state and (c)  $|^2N(56, 2^+)_{\frac{1}{2}^+} \rangle$  state with the notation  $|^{2J+1}N(N_6, N^P)J^P \rangle$ , where  $J$ ,  $N_6$ ,  $N$  and  $P$  denote the total angular momentum, the dimension of  $SU_{SF}(6)$  group, the principal quantum number and the parity of the state, respectively. The solid and dashed curves correspond to the  $\Delta$ -mode confining potential and the  $Y$ -mode confining potential cases, respectively.

induced quark-quark interaction is introduced through the interaction Lagrangian

$$\mathcal{L}_I^v = -g_{chv} \bar{\psi} \gamma_\mu T^a A_a^\mu \psi - \frac{f_{chv}}{2M_P} \bar{\psi} \sigma_{\mu\nu} T^a \partial^\nu A_a^\mu \psi, \quad (29)$$

where  $g_{chv}$  and  $f_{chv}$  are the coupling constants for the vector coupling and the tensor coupling, respectively. The form of the additional potential can be written as

$$V_{ij}^v = \sum_{a=0}^8 V_{\rho_a}(r_{ij}), \quad (30)$$

where  $\rho_0, \dots, \rho_8$  denote the singlet and octet vector fields, and

$$V_{\rho_a}(r_{ij}) = C(g_{chv}, m_{\rho_a}, \Lambda) \left\{ X_1(m_{\rho_a}, \Lambda, r_{ij}) + \frac{m_{\rho_a}^2}{6m_{q_i}m_{q_j}} \left( 1 + \frac{f_{chv}}{g_{chv}} \frac{m_{q_i} + m_{q_j}}{M_P} + \frac{f_{chv}^2}{g_{chv}^2} \right. \right. \\ \left. \left. \times \frac{m_{q_i}m_{q_j}}{M_P^2} \right) X_2(m_{\rho_a}, \Lambda, r_{ij})(\sigma_i \cdot \sigma_j) \right\} [\lambda_a(i)\lambda_a(j)] + V_{\rho_a}^{l.s}(r_{ij}) + V_{\rho_a}^{ten}(r_{ij}), \quad (31)$$

$$V_{\rho_a}^{l.s}(r_{ij}) = -C(g_{chv}, m_{\rho_a}, \Lambda) \frac{3m_{\rho_a}^2}{4m_{q_i}m_{q_j}} \left( 1 + \frac{f_{chv}}{g_{chv}} \frac{2(m_{q_i} + m_{q_j})}{3M_P} \right) \\ \times \left\{ G(m_{\rho_a}r_{ij}) - \left( \frac{\Lambda}{m_{\rho_a}} \right)^3 G(\Lambda r_{ij}) \right\} [L \cdot (\sigma_i + \sigma_j)][\lambda_a(i)\lambda_a(j)], \quad (32)$$

$$V_{\rho_a}^{ten}(r_{ij}) = -C(g_{chv}, m_{\rho_a}, \Lambda) \frac{m_{\rho_a}^2}{12m_{q_i}m_{q_j}} \left( 1 + \frac{f_{chv}}{g_{chv}} \frac{m_{q_i} + m_{q_j}}{M_P} + \frac{f_{chv}^2}{g_{chv}^2} \frac{m_{q_i}m_{q_j}}{M_P^2} \right) \\ \times \left\{ H(m_{\rho_a}r_{ij}) - \left( \frac{\Lambda}{m_{\rho_a}} \right)^3 H(\Lambda r_{ij}) \right\} \hat{S}_{ij}[\lambda_a(i)\lambda_a(j)], \quad (33)$$

with  $m_{\rho_a}$  being the mass of the vector meson.

In the extended model, some additional parameters are introduced [3]. Based on  $g_{NN\rho}$  value in the phenomenological  $NN$  interaction model, the coupling constants  $g_{chv}$  and  $f_{chv}$  can be estimated as  $g_{chv} = 2.351$  and  $f_{chv} = 2/3g_{chv}$ , respectively. The mixing angle between  $\omega_1$  and  $\omega_8$  is taken to be  $\theta^V = 35.26^\circ$ , which indicates an ideal mixtrue. The model parameters are summarized in Table VI.

In the chiral SU(3) quark model, we find that the baryon spectra in the  $\Delta$ -mode and the Y-mode confining potential cases are rather close, and that one cannot definitely distinguish which confining mode is better through the spectra only because the mass of baryon is closely related to the averaged value of the confining potential operator. Therefore, in order to see whether a reasonable description for baryon spectra can be obtained in the extended chiral SU(3) quark model also, we calculate the baryon spectra with the  $\Delta$ -mode only. The baryon spectra for  $S = 0, -1, -2, -3$  in the extended chiral SU(3) quark model are plotted in Figs.9-11. In these figures, the solid and dashed bars denote the results with and without the tensor coupling in the vector meson potential, respectively. The fitting quality in the extended model is close to that in the chiral SU(3) quark model except for a few states, and the deviations between the states with vector coupling of the vector meson potential only and those with both vector and tensor couplings of the vector meson potential are very small. The resultant mass of Roper resonance ( $N(\frac{1}{2}^+, 1440)$ ) is 25 MeV smaller than that in the chiral SU(3) quark model. It is even closer to the experimental value, but



TABLE VI: Parameters of extended chiral SU(3) quark model. The vector meson masses  $m_\rho = 770MeV$ ,  $m_{K^*} = 892MeV$ ,  $m_\omega = 782MeV$ ,  $m_{K^*} = 1020MeV$  and the cutoff momentum  $\Lambda = 1100MeV$ . (1) $f_{chv} = 0$ , (2) $f_{chv} \neq 0$ .

Extended chiral SU(3) quark model		
	(1)	(2)
$\omega(MeV)$	497.6	497.6
$g_{ch}$	2.621	2.621
$g_{chv}$	2.351	1.972
$f_{chv}/g_{chv}$	–	2/3
$m_\sigma(MeV)$	535	547
$g_u$	0.521	0.598
$g_s$	0.545	0.614
$b_{uu}(GeV/fm)$	0.57	0.58
$b_{us}(GeV/fm)$	1.03	0.99
$b_{ss}(GeV/fm)$	2.01	2.04
$c_{uu}(MeV)$	-566	-524
$c_{us}(MeV)$	-855	-769
$c_{ss}(MeV)$	-1285	-1224

is still larger than the first orbital resonance ( $N(\frac{1}{2}^-, 1535)$ ). Moreover, in the extended model, the level intervals among  $\Lambda(\frac{1}{2}^-)$  states become larger.

It should be mentioned that because the effect of the vector meson exchange can partially replace the role of the one gluon exchange, introducing vector meson exchange potential can reduce the strong coupling constant  $\alpha_s$  to some extent, which is desirable by QCD expectation.

#### IV. NONSTRANGE BARYON STRONG DECAY

A successful hadron model should be able to explain as much data as possible such as the spectrum, magnetic moments, decay width and etc.. The chiral SU(3) quark model is quite successful in reproducing the experimental data of the hadron-hadron scattering and baryon spectrum. Now, we would check if this model can give a reasonable description of the strong decay width of non-strange baryon resonances.

As well known, the theory of a baryon strongly decay into hadrons is far away from establishment. In this section, we use a simple model, called the point-like meson emission model, to estimate the decay width of the  $N^* \rightarrow NM$  process. In this model, the baryon has its own quark structure, and the point-like meson is emitted from one of the quarks in baryon (see Fig. 12).

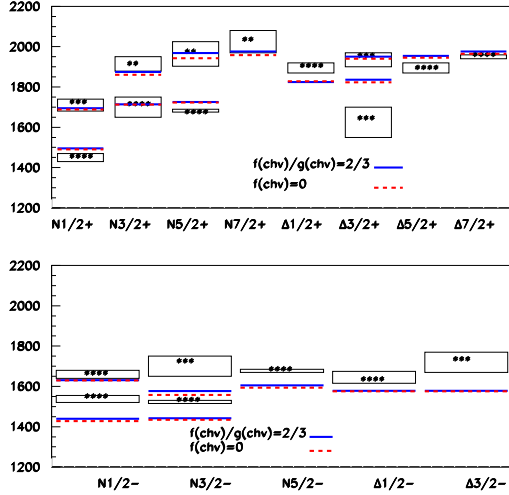


FIG. 9: The non-strange baryon spectra in  $N \leq 2$  bands in the extended chiral SU(3) quark model. The solid and dashed bars represent the results with and without the tensor coupling, respectively.

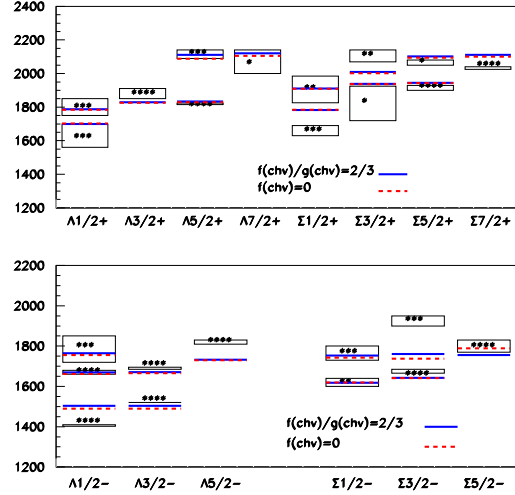


FIG. 10: The S=-1 baryon spectra in  $N \leq 2$  bands in the extended chiral SU(3) quark model. Legend as in Fig.9.

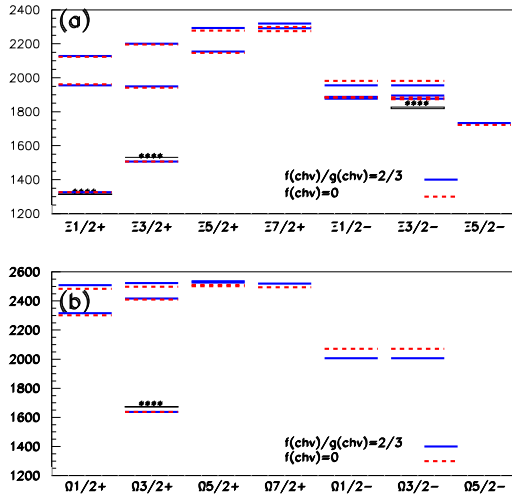


FIG. 11: The S=-2,-3 baryon spectra in  $N \leq 2$  bands in the extended chiral SU(3) quark model. Legend as in Fig.9.

The amplitude responsible for the emission of a pseudoscalar meson is usually assumed as

$$\begin{aligned}
 \langle NM | H_s | N^* \rangle &= \sum_{i=1}^3 \langle N e^{-i\mathbf{k}\cdot\mathbf{r}_i} | (x\mathbf{k}\cdot\sigma_i + y\mathbf{p}_i\cdot\sigma_i) X_{i,M} | N^* \rangle \\
 &= 3 \langle N e^{-i\mathbf{k}\cdot\mathbf{r}_1} | (x\mathbf{k}\cdot\sigma_1 + y\mathbf{p}_1\cdot\sigma_1) X_{1,M} | N^* \rangle,
 \end{aligned} \tag{34}$$

where the factor 3 is due to the symmetry of the wave function of three identical quarks,  $\mathbf{k}$  is the

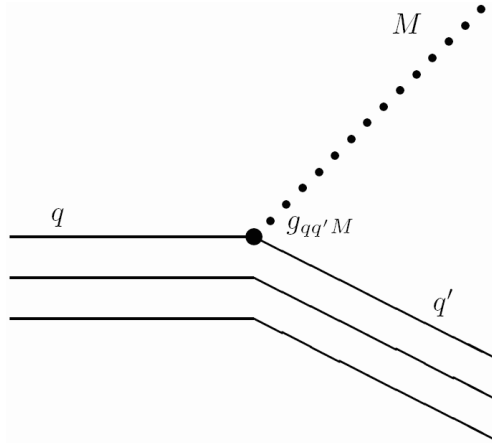


FIG. 12:  $B^* \rightarrow B M$  decay in the point-like meson emission model.

momentum of the emitted meson,  $\mathbf{r}_i$ ,  $\mathbf{p}_i$ ,  $\frac{1}{2}\sigma_i$  and  $X_{i,M}$  are the coordinate, the momentum, the spin and the flavor matrix, that describe the quark transition process  $q_i \rightarrow q'_i + M$ , of the  $i$ -th quark, respectively, and  $x$  and  $y$  are phenomenological constants. For neutral-pion emission,  $X_M$  can be written as

$$X_{\pi^0} = \lambda_3, \quad (35)$$

where  $\lambda_3$  is the Gell-Mann matrix. The wave function of the  $|N^*\rangle$  state is obtained by the configuration mixing in calculating the spectrum in the chiral SU(3) quark model.

In the center of mass frame of the non-strange baryon, the width of a non-strange baryon decaying into a ground state nucleon and a  $\pi$  meson can be written as

$$\Gamma_{N\pi} = \frac{1}{\pi} \frac{|\langle f | \mathcal{H}_s | i \rangle|^2 k E_N}{2J_R + 1 m_R} \langle I_N, I_{3N}, I_\pi, I_{3\pi} | I_{N^*}, I_{3N^*} \rangle^{-2}, \quad (36)$$

where  $J$ ,  $I$  and  $I_3$  represent the total angular momentum, the isospin and the third component of isospin, respectively.

In Table VII, we show the calculated decay width  $\Gamma_{N\pi}^{1/2} (MeV^{1/2})$  of a four-star or a three-star non-strange resonance decaying into a nucleon and a pion. For comparison, the results in [28] are also listed in the table VII. The parameters  $x$  and  $y$  are obtained by a  $\chi^2$  fit. From the table, one sees that most of the decay widths in our model agree with the experimental data and are comparable to those in Ref. [28]. The decay widths of  $N(\frac{1}{2}^+, 1440)$  and  $N(\frac{1}{2}^-, 1535)$  deviate from the data greatly, because the order of the masses of these two resonances in the model prediction are opposite down. Moreover, the corresponding decay widths in two confining mode cases are also very close because the corresponding wave functions are very close.

TABLE VII: Square root of the non-strange baryon decay widths,  $\Gamma_{N\pi}^{1/2}$ , in  $\text{MeV}^{1/2}$ , together with the parameter  $x$  and  $y$ . Column 3 are the results from [28]. Column 3 and 4 correspond to  $\Delta$ -shape and Y-shape confining potential and the last column are experimental data from [23].

	Isgur	$\Delta - shape$	Y-shape	Expt.
$x(\text{fm})$		$0.752 \times 10^{-2}$	$0.743 \times 10^{-2}$	
$y(\text{fm})$		$-0.845 \times 10^{-4}$	$-0.217 \times 10^{-3}$	
Resonance	$\Gamma_{N\pi}^{1/2}(\text{MeV}^{1/2})$			
$N_{\frac{1}{2}}^{-}(1535)$	5.3	13.2	13.3	$8.2 \pm 2.3$
$N_{\frac{1}{2}}^{-}(1650)$	8.7	8.6	8.2	$10.4 \pm 2.0$
$N_{\frac{3}{2}}^{-}(1520)$	9.2	11.5	10.9	$8.1 \pm 0.8$
$N_{\frac{3}{2}}^{-}(1700)$	3.6	2.9	2.9	$3.2 \pm 1.6$
$N_{\frac{5}{2}}^{-}(1675)$	5.5	6.7	6.4	$8.2 \pm 1.0$
$N_{\frac{1}{2}}^{+}(1440)$	6.8	6.6	6.1	$15.1 \pm 2.8$
$N_{\frac{1}{2}}^{+}(1710)$	6.7	3.1	3.2	$3.9 \pm 2.4$
$N_{\frac{3}{2}}^{+}(1720)$	6.5	3.4	3.8	$4.7 \pm 1.6$
$N_{\frac{5}{2}}^{+}(1680)$	7.1	2.4	2.6	$9.2 \pm 0.7$
$\Delta_{\frac{1}{2}}^{-}(1620)$	3.3	5.7	5.7	$6.1 \pm 1.2$
$\Delta_{\frac{3}{2}}^{-}(1700)$	4.9	6.4	6.9	$6.7 \pm 2.2$
$\Delta_{\frac{1}{2}}^{+}(1910)$	5.3	5.7	4.9	$7.5 \pm 1.8$
$\Delta_{\frac{3}{2}}^{+}(1232)$	10.2	10.3	10.7	$10.9 \pm 0.2$
$\Delta_{\frac{5}{2}}^{+}(1905)$	4.0	5.5	5.7	$5.9 \pm 2.2$
$\Delta_{\frac{7}{2}}^{+}(1950)$	7.5	10.6	10.4	$10.6 \pm 0.9$

## V. CONCLUSIONS

The baryon spectra with both Y-mode and  $\Delta$ -mode confining potentials in  $N \leq 2$  bands are studied in the chiral  $SU(3)$  quark model. The results show that, no matter which type of confining potential, say the  $\Delta$ -mode or the Y-mode or even the mixed mode, is employed, the experimental baryon spectra can be well-explained. The resultant baryon spectra with the Y-mode and  $\Delta$ -mode confining potentials are very close to each other. For most of the states, the corresponding mass difference with different confining modes is less than 20 MeV. Moreover, the  $\Delta$ -mode confinement is more effective in the short and medium distances and the Y-mode confinement provides more contributions in the long distance. It is also shown that the effect of the different confining mode does not distinctly show up in the spectrum. The strong decay widths of the non-strange baryon resonances are calculated in the point-like meson emission model with the wave-functions obtained in the baryon spectrum calculation. The resultant decay widths are generally in agreement with the experimental data. However, this mode is too simple. The detailed decay information of baryons should be extracted from the investigation in the implicit quark-gluon degrees of freedom.

This work is partially supported by the National Natural Science Foundation of China under grant Nos. 10475089, 10435080, 10375090 and CAS grant No. KJCX3-SYW-N2.

- 
- [1] F. Fernandez, A. Valcarce, U. Straub, A. Faessler, J. Phys. **G19**, 2013 (1993).
- [2] Z.Y. Zhang, Y.W. Yu, P.N. Shen, L.R. Dai, A. Faessler, U. Straub, Nucl. Phys. A **625**, 59 (1997).
- [3] L.R. Dai, Z.Y. Zhang, *et al.*, Nucl. Phys. A **727**, 321 (2003).
- [4] F. Huang, Z.Y. Zhang, Y.W. Yu, B.S. Zou, Phys. Rev. C **70**, 064004 (2004).
- [5] Q.B. Li, P.N. Shen, Z.Y. Zhang, Y.W. Yu, Nucl. Phys. A **683**, 487 (2001).
- [6] F. Huang, Z.Y. Zhang, Y.W. Yu, B.S. Zou, Phys. Lett. B **586**, 69 (2004).
- [7] H.M. Zhao, P.N. Shen, Y.B. Ding, X.Q. Li, B.S. Zou, Commu. in Theor. Phys. **46**, 275 (2006).
- [8] J. Carlson *et al.*, Phys. Rev. **D27**, 233 (1983);  
D. Gromes and I. O. Stumatescu, N. P. **B112**, 213 (1976).
- [9] N. Isgur, J. Paton, Phys. Rev. **D31**, 2809 (1985).
- [10] G. S. Bali, K. Schilling, *Como 1996, Quark confinement and the hadron spectrum II*, 277 (1996).
- [11] T. T. Takahashi *et al.*, Phys. Rev. Lett. 86(2001)18; Phys. Rev. D 65(2002)114509.
- [12] S. Capstick and N. Isgur, Phys. Rev. **D34**, 2809 (1986).
- [13] J. Kogut and L. Susskind, Phys. Rev. **D11**, 395 (1975)
- [14] C. Alexandrou, ph de Forcrand and A. Tsapalis, Phys. Rev. D65(2002)054503; Nucl. Phys. Proc. Suppl., 109A(2002)153.
- [15] S. Pepin and Fl. Stancu, Phys. Rev. D65(2002)054032;
- [16] D. S. Kuzmenko, Phys. Atom. Nucl. 67(2004)548.
- [17] I. N. Narodetskii and M. A. Trusov, Phys. Atom. Nucl. 67(2004)762.
- [18] N. Brambilla, G. M. Prospero and A. Vairo, Phys. Lett. B362(1995)113.
- [19] I.T. Obukhovskiy and A.M. Kusainov, Phys. Lett. B **238**, 142 (1990).
- [20] A.M. Kusainov, V.G. Neudatchin, and I.T. Obukhovskiy, Phys. Rev. C **44**, 2343 (1991).
- [21] D. Flamm, Introduction to the quark model of elementary particles (Gordon and Breach 1982).
- [22] F.E. Close, An introduction to quarks and partons, (Academic Press London 1979).
- [23] Particle Data Group, Phys. Lett. B **592**, 1 (2004).
- [24] N. Isgur, G. Karl, Phys. Rev. D 18 (1978)418;  
N. Isgur, G. Karl, Phys. Rev. D 19 (1979)2653.
- [25] P.R. Page, *Hybrid Baryons*, 9th International Conference on the Structure of Baryons (BARYONS 2002), 3-8 March, Newport News, VA, USA. (nucl-th/0204031), B.S. Zou and D.O. Riska, Phys. Rev. Lett. **96**, 072001(2005); B.C. Liu and B.S. Zou, Phys. Rev. Lett. **96**, 042002(2006).
- [26] Y.W. Yu, Z.Y. Zhang, High Energy Phys. and Nucl. Phys. **28**, 594 (2004).
- [27] L.R. Dai, Z.Y. Zhang, *et al.*, Nucl. Phys. A **727**, 321 (2003).

[28] R. Koniuk, N. Isgur, Phys. Rev. D 21 (1980)1868.

